Electronic Supplementary Material (ESI) for Physical Chemistry Chemical Physics.

Supporting Information

Experimental validation of 'Pnicogen Bonding' in Nitrogen from charge density analysis

Sounak Sarkar, Mysore S. Pavan and T. N. Guru Row*

Solid state and Structural Chemistry Unit,

Indian Institute of Science, Bangalore 560012, India

S-1: Experimental section including data collection, structure refinement, multipole modeling and computational details

F-1: ORTEP diagram of the molecule

T-1: Crystallographic table of the experimental structure

F-2: (a) Variation of Fobs/Fcal with (sinθ)/λ (b) Scatter plot depicting the variation of Fobs with Fcal for (**I**)

T-2: Topological parameters of intramolecular bonds from Experiment

T-3: Topological parameters of intramolecular bonds from Theory

S-2: CSD Analysis

T-4: Summary of CSD Analysis

F-3: Histograms depicting various N•••X distance distribution along with corresponding scatter plots showing the N•••X distance vs. X–N•••X angle.

F-4: Histogram depicting the N-H•••X angle distribution of the possible bifurcated H-bonding in (**I**)

T-5: Structures found in the CSD analysis having biological relevance

F-5: Fractal dimension plot of experimental and theoretical model (a) & (b) (**I**)

F-5: Probability distribution plot of experimental model

F-6: Experimental and Theoretical residual density, Laplacian and 2D deformation maps.

F-7: Comparison between experiment and theory AIM charges

F-8: Theoretical bond paths together with bcp's in the intermolecular regions of (**I**)

S-1: Experimental Section

Crystallization: 2-Amino-5-nitropyridine and chloroacetic acid were taken in 1:1 molar ratios in mortar pastel and ground well with addition of few drops of methanol. The resulting solid was kept for crystallization in saturated solution of methanol at low temperature. Good quality single crystals were chosen using a polarizing microscope and affixed to a Hampton Research Cryoloop using Paratone-N oil.

Data collection and structure refinement details

A crystal of dimensions 0.4 × 0.2 × 0.1 mm, was cooled to 100 K with a liquid nitrogen stream using an Oxford Cryostream nitrogen gas-stream cooling device. X-ray diffraction data was collected on an Oxford Xcalibur (Mova) diffractometer[1]equipped with an EOS CCD detector using *MoKα* radiation (λ= 0.71073 Å). The crystal to detector distance was fixed at 45 mm and the scan width (Δω) was 1° per frame during the data collection. The data collection strategy was chosen in such a way to yield a high resolution X-ray data set (d= 0.45 Å), with a high redundancy (~12) and completeness of 100%. Cell refinement, data integration and reduction were carried out using the program CrysAlisPro.[1] Face indexing was done to facilitate accurate numerical absorption correction. Sorting, scaling, and merging of the data sets were carried out using the program SORTAV.[2] The crystal structure was solved by direct method using SHELXS97and refined based on the spherical-atom approximation (based on F2) using SHELXL97[3] included in the WinGX package suite.[4] The hydrogen atom was located on the difference Fourier map and its position and isotropic thermal parameters were allowed to refine in the spherical atom model.

Multipole Modeling

The charge density modeling and multipolar aspherical atom refinements were performed based on the Hansen and Coppens multipole formalism using XD2006.[5] The function, Σw^2 was minimized for all reflections with $I > 2\sigma(I)$. Weights (w) were taken as $1/\sigma^2$ (Fo^2) and convergence criterion of the refinement was set to a maximal shift/esd $<10^{-10}$. Su-Coppens-Macchi wave functions [6] were used for the core and valence scattering factors of all the atoms. Scale factors for each individual resolution shell were chosen (10 scale factors) and refined against the entire resolution range of diffraction data in the first refinement step. The scatter plot of the variation of F_{obs} with F_{cal} is indicative of the quality of the data set after scaling. The positional and anisotropic displacement parameters of the non-hydrogen atoms were refined using reflection data with $\sin\theta/\lambda > 0.7$ Å^{-1}. Since the space group of (**I**) was *Cc*, the origin was fixed on the Chlorine atom. In the next step of refinement, the position and displacement parameters of the non-hydrogen atoms were fixed to the refined values. The X—H bond lengths were constrained to the values reported by neutron diffraction experiments in literature.[7] The isotropic displacement parameters of the H-atom was refined initially with reflection data $\sin\theta/\lambda < 0.7$ Å^{-1}. Further, the converged model was used to calculate anisotropic displacement parameters of H-atom using the SHADE2.1 server. [8] ADP value of the H-atom obtained from SHADE2.1 server was kept fixed during the subsequent multipole refinements.[9] Then the scale, positional and anisotropic displacement parameters, P_{val}, P_{lm}, and on non-hydrogen atoms were refined in a stepwise manner, until the convergence criterion was reached. Separate κ and κ' were used to define different non-H atom type based chemical environments, while for the

hydrogen atoms the value was fixed at 1.2. All the atoms in (**I**) were refined with an unrestricted multipole model. The multipole expansion was truncated upto hexadecapole level (l = 4) for only chlorine in (**I**), where as for other non-hydrogen atoms it was truncated at the octupole level (l = 3) in both cases. For the H atoms, only monopole, bond directed dipole (dz) and quadrupole (q_{3z^2-1}) components were refined during the multipole refinements. The multipole refinement was done keeping anisotropic harmonic model. The quantitative analysis of the electron density topology and related properties was performed using the XDPROP and TOPXD[10] module of XD software suite.[5] Crystallographic refinement details of both spherical and multipolar model are summarized in Table 1.

Computational details

Theoretical Charge Density

Positional parameters obtained from the experimental charge density model have been used for density functional calculations using the hybrid exchange correlational functional B3LYP[11] with TZVP basis set [12] included in CRYSTAL09 package.[13] The shrinking factors (IS1, IS2, and IS3) and the reciprocal lattice vectors were set to 3 (with 10 k-points in irreducible Brillouin zone). The bielectronic Coulomb and exchange series values for the truncation parameter were set as ITOL1_ITOL4 = 6 and ITOL5 = 12, respectively, for the calculations. The level shifter was set to 0.3 Hartree/cycle as 30% mixing of Fock/KS matrices (FMIXING) given in the input. An SCF convergence limit of the order of 10-6 Hartree was used In the static model, atomic thermal displacement parameters for all atoms were set to zero.

Structure factors were calculated for a resolution of 1.08$Å^{-1}$, which were used for the theoretical multipolar model. Refinements and analysis for the theoretical charge density model were performed using the XD software package following the same methodology used for the experimental charge density modeling.

NBO Calculation

The Natural Bond Orbital (NBO) method[14] has been used to analyze the 'pnicogen bonding' in (**I**) .The analysis of the off-diagonal elements of the Fock matrix by second-order perturbation theory shows two interactions between two monomeric units (Clacac and 2-A5NP) as there is a stabilizing charge transfer from the three lone pair orbitals of Cl (LP (1)), LP (2)) and (LP (3)) atom in donor Chloroacetic acid (Clacac) into the anti-bonding σ* orbital of N-C bond (BD* (1) N-C) of acceptor of 2-Amino-5-Nitropyridine(2-A5NP).The NBO calculations are carried out on (**I**) and also on Clacac and 2-A5NP separately as implemented in Gaussian09[15] at wB97XD[16] with a basis set of TZVP.[17] The inputs for the single point calculations are derived from the multipole model of (**I**). The outputs from the NBO calculation are viewed using Chemcraft 1.7.[18]

Table 2 in the manuscript lists the details of the outcome from the NBO analysis. The conclusions can be made (**Table 2**) on the account of orbital energy and orbital occupancy changes of the participating orbitals in N···Cl pnicogen bonding interaction. For instance in (**I**) the energies of all the lone pair natural bond orbitals (LP (1)), LP (2)) and (LP (3)) decreases with respect to their values in the monomer (Clacac), as the orbitals are becoming stabilized with a subsequent decrease in their occupancies. Contrariwise is encountered for acceptor σ*C-N antibonding orbital in terms of orbital energy and orbital occupancy with respect to its monomeric counterpart.

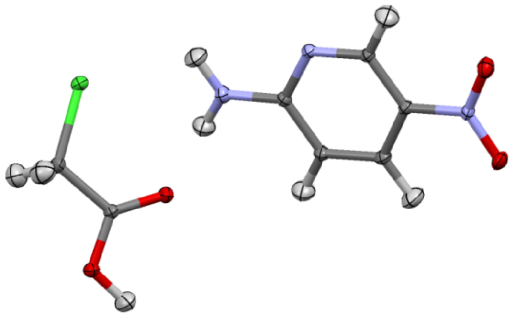

Figure 1: Ortep diagram of co-crystal of 2-amino-5-nitropyridine and chloroacetic acid. (**I**)

Table 1: Crystallographic table of the experimental structure

Compound	(**I**)
CCDC	1019123
Chemical formula	$C_5H_5N_3O_2{\cdot}C_2H_3ClO_2$
Molecular formula	233.61
Crystal system, space group	Monoclinic, *Cc*
Temperature (K)	100(2)
a, *b*, *c* (Å)	4.8198 (1), 21.7824 (3), 9.3616 (2)
β (°)	104.264 (2)
V (Å^3)	952.54 (3)
Z	4
ρ_{calc} *(g/cm^3)*	1.628
T(K)	100(2)
F(000)	480
λ(Å)	0.71073
$(\sin\theta/\lambda)_{max}$ (Å^{-1})	1.080
Radiation type	Mo *K*α
μ (mm^{-1})	0.40
Crystal size (mm)	0.42 × 0.18 × 0.11
Data collection	
Absorption correction	Gaussian
T_{min}, T_{max}	0.883, 1.678
Measured, independent and observed [$I > 2\sigma(I)$] reflections	52653, 9688, 8542
R_{int} (%)	4.4
$(\sin\theta/\lambda)_{max}$ (Å^{-1})	1.080
Spherical Refinement	
$R[F^2 > 2\sigma(F^2)]$, $wR(F^2)$, S	0.033, 0.078, 1.05
No. of unique reflections	9688
Completeness (%)	96.3
Redundancy	5.4
No. of restraints	10
$\Delta\rho_{max}$, $\Delta\rho_{min}$ (e Å^{-3})	0.64, −0.25
Absolute structure parameter	0.03 (2)
Multipole Refinement	
Reflns.used[I>2σ(I)]	8542
No of parameters	446
R (F^2)	0.0327
wR $_2$ (F^2)	0.0446
Goodness-of-fit	0.9060
$\Delta\rho_{min,max}$(eÅ^{-3})	-0.233,0.215

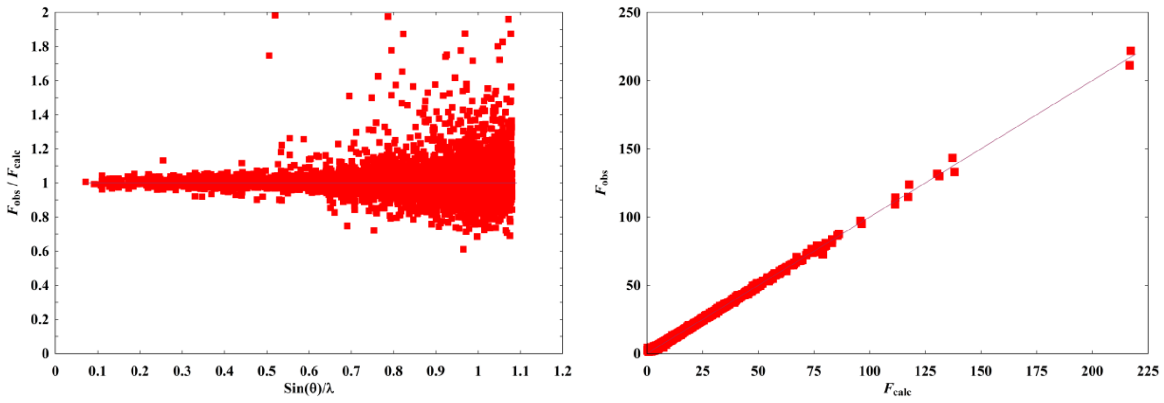

Figure 2: (a) Variation of Fobs/Fcal with (sinθ)/λ (b) Scatter plot depicting the variation of Fobs with Fcal for (**I**)

Table 2: Topological parameters of intramolecular bonds from Experiment

Bond	ρ (eÅ^{-3})	$\nabla^2\rho$(eÅ^{-5})	R_{ij} (Å)	λ_1	λ_2	λ_3	ε
CL(1)-C(1)	1.17(3)	0.17(5)	1.7786	-6.46	-5.75	12.38	0.12
O(1)-C(2)	2.62(4)	-36.0(2)	1.2953	-24.35	-22.52	10.91	0.08
O(1)-H(1O)	1.54(9)	-29.4(8)	1.018	-29.14	-28.86	28.63	0.01
O(2)-C(2)	3.01(5)	-43.7(3)	1.2303	-32.43	-27.19	15.93	0.19
O(3)-N(1)	3.33(4)	-7.1 (1)	1.2316	-30.88	-29.00	52.73	0.07
O(4)-N(1)	3.26(4)	-6.3(1)	1.2311	-30.81	-27.71	52.17	0.11
N(1)-C(6)	1.94 (4)	-13.1(1)	1.4436	-15.59	-11.99	14.51	0.3
N(2)-C(3)	2.46(5)	-25.9(2)	1.3322	-21.87	-17.86	13.79	0.22
N(2)-H(2A)	2.23(1)	-30.0(6)	1.011	-31.26	-29.15	30.46	0.07
N(2)-H(2B)	2.1(1)	-27.8 (7)	1.0115	-29.30	-28.06	29.55	0.04
N(3)-C(3)	2.34(4)	-21.2(1)	1.3575	-20.00	-16.73	15.55	0.2
N(3)-C(7)	2.33(4)	-21.0(1)	1.3405	-18.86	-17.27	15.11	0.09
C(1)-C(2)	1.73(3)	-12.36(7)	1.519	-12.86	-10.97	11.47	0.17
C(1)-H(1A)	1.77(9)	-15.2 (4)	1.0913	-16.53	-15.87	17.2	0.04
C(1)-H(1B)	1.86 (8)	-19.1(4)	1.0912	-17.90	-17.14	15.94	0.04
C(3)-C(4)	2.06(3)	-17.09(9)	1.424	-16.07	-13.10	12.08	0.23
C(4) -C(5)	2.21(4)	-18.9(1)	1.3711	-17.40	-13.58	12.06	0.28
C(4)-H(4)	1.92 (9)	-20.3(4)	1.0838	-18.36	-17.31	15.4	0.06
C(5)-C(6)	2.15(4)	-18.02(9)	1.4042	-16.95	-13.38	12.32	0.27
C(5)-H(5)	1.74(9)	-14.2(4)	1.0823	-16.6	-15.99	18.37	0.04
C(6)-C(7)	2.19(4)	-20.49(9)	1.3782	-17.62	-14.23	11.36	0.24
C(7)-H(7)	1.97(9)	-19.5(4)	1.0829	-19.33	-17.80	17.68	0.09

Table 3: Topological parameters of intramolecular bonds from Theory

Bond	ρ (eÅ^{-3})	$\nabla^2\rho$(eÅ^{-5})	R_{ij} (Å)	λ_1	λ_2	λ_3	ε
CL(1)-C(1)	1.097(4)	1.222(7)	1.7777	-5.56	-5.49	12.27	0.01
O(1)-C(2)	2.346(6)	-23.47 (3)	1.295	-20.16	-18.11	14.79	0.11
O(1)-H(1O)	1.90 (1)	-16.75(5)	1.0186	-26.45	-26.06	35.76	0.02
O(2)-C(2)	2.795(7)	-33.53 (3)	1.2302	-26.00	-22.5	14.97	0.16
O(3)-N(1)	2.900(7)	3.25 (2)	1.2311	-24.26	-22.71	50.22	0.07
O(4)-N(1)	2.911(7)	0.84 (2)	1.2308	-24.77	-23.91	49.52	0.04
N(1)-C(6)	1.739(5)	-7.52 (2)	1.4432	-13.73	-10.64	16.84	0.29
N(2)-C(3)	2.327(7)	-19.06 (2)	1.3321	-19.34	-16.12	16.4	0.2
N(2)-H(2A)	2.155(9)	-22.16(4)	1.0109	-27.51	-25.29	30.65	0.09
N(2)-H(2B	2.12 (1)	-21.29(5)	1.0111	-26.94	-25.16	30.81	0.07
N(3)-C(3)	2.235(6)	-15.65(2)	1.3581	-17.15	-15.61	17.11	0.1
N(3)-C(7)	2.243(5)	-15.82 (2)	1.3404	-16.89	-15.58	16.65	0.08
C(1)-C(2)	1.734(4)	-11.373(9)	1.5176	-12.38	-11.47	12.48	0.08
C(1)-H(1A)	1.789(8)	-15.58(2)	1.0914	-16.37	-16.1	16.9	0.02
C(1)-H(1B	1.788(8)	-15.53 (2)	1.0916	-16.71	-16.55	17.73	0.01
C(3)-C(4)	1.964(4)	-14.28(1)	1.4239	-14.36	-12.39	12.48	0.16
C(4)-C(5)	2.125(5)	-16.22(2)	1.3709	-16.07	-12.77	12.61	0.26
C(4)-H(4)	1.797(9)	-15.27(3)	1.0825	-16.91	-16.05	17.7	0.05
C(5)-C(6)	2.051(5)	-16.232(2)	1.4047	-15.84	-13.25	12.86	0.2
C(5)-H(5)	1.836(8)	-15.65(2)	1.0824	-17.53	-16.79	18.67	0.04
C(6)-C(7)	2.208(5)	-19.95(1)	1.3783	-17.43	-14.94	12.42	0.17
C(7)-H(7)	1.866(9)	-17.142(3)	1.0826	-17.93	-17.8	18.59	0.01

S-2: CSD Analysis

Table 4: Summary of CSD Analysis

Pnicogen bond acceptor atom (X)	**Number of entries**	**Mean N•••X distance (Å)**	**Mean X–N•••X angle,θ(°)**
O	252	2.952	170.411
N	59	3.011	171.168
F	14	2.920	170.539

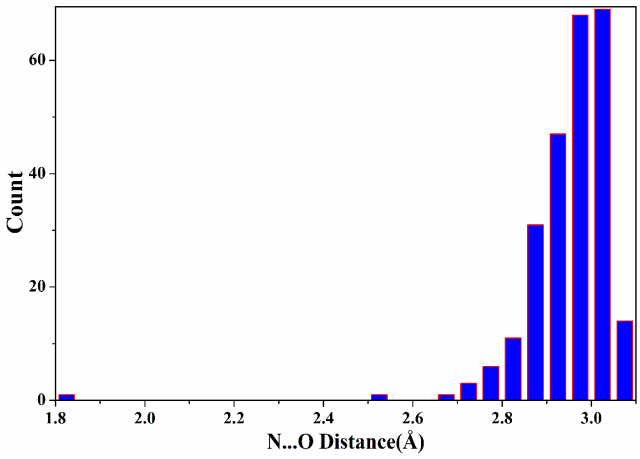
Count
N...O Distance(Å)

(a)

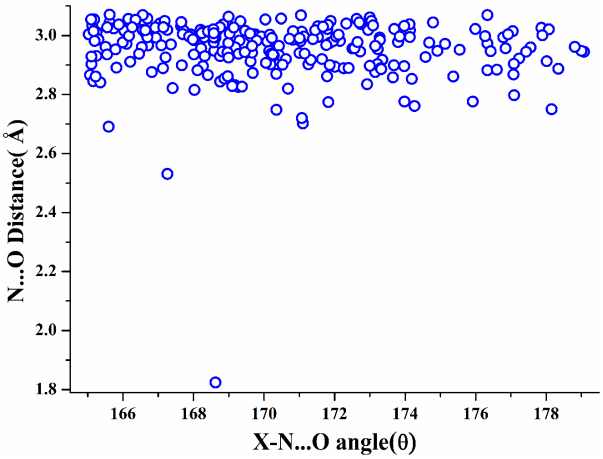
N...O Distance(Å)
X-N...O angle(θ)

(b)

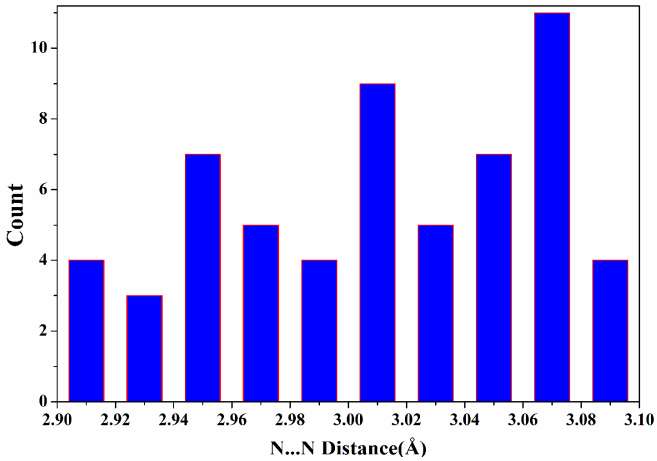
Count
N...N Distance(Å)

(c)

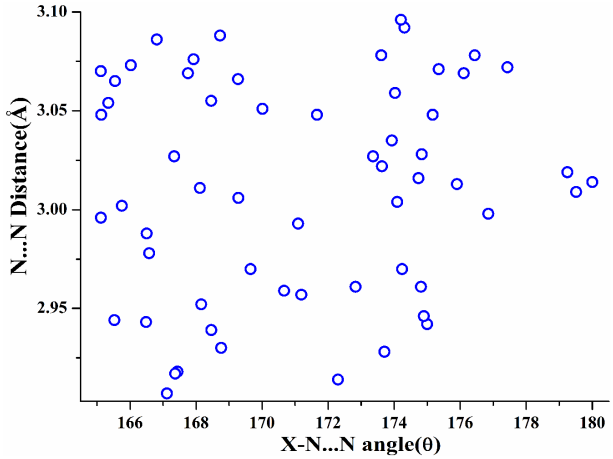

(d)

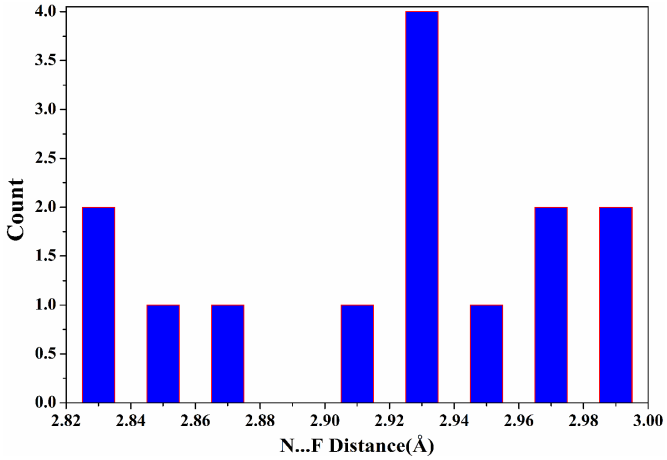

(e)

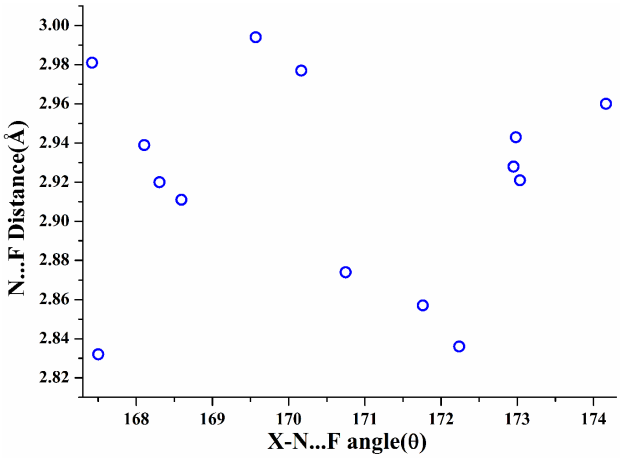

(f)

Figure 3(a-f): Histograms depicting various N•••X distance distribution along with corresponding scatter plots showing the N•••X distance vs. X–N•••X angle.

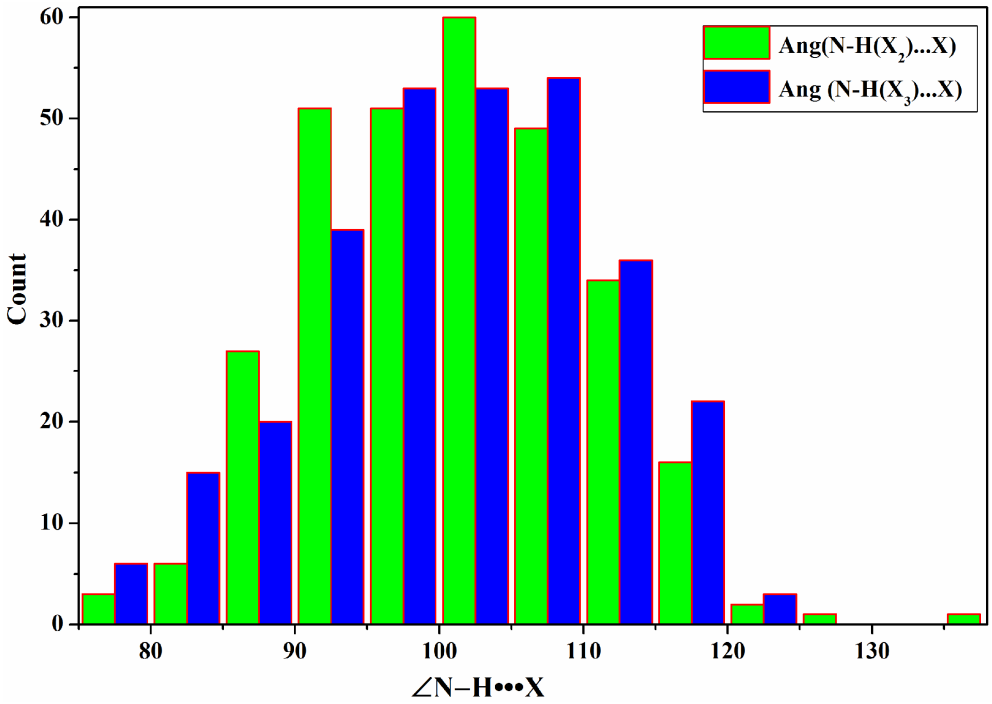

Figure 4: Histogram depicting the N-H•••X angle distribution of the possible bifurcated H-bonding in (**I**)

Table 5: Structures found in the CSD analysis having biological relevance

Refcode	Compound Name (L)	Biological Activity
ATDZSA01	5-Acetamido-1,3,4-thiadiazole-2-sulfonamide	drug used for treatment of glaucoma and epilepsy and also a diuretic
BIXMIF	Sulfamic acid 2-bromo-4-•••4-cyanophenyl)(1,2,4-triazol-4-yl)amino)methyl)phenyl ester ethyl acetate solvate	sulfatase inhibitor (DASI) in JEG-3 cells
BOLMAR	5-Fluorouracil formamide solvate	is an anticancer agent
DPGUAN03	N,N'-Diphenylguanidine	cure accelerator in the rubber industry
DUPFAV	Deamino-oxytocin heptahydrate	neurohypophyseal hormonal agent
EMIKOA	2-Amino-6-(1-imidazolylmethyl)-4-(3,5,5-trimethyl-2-pyrazolin-1-yl)-1,3,5-triazine	potential biological activity
EMIKUG	2-Amino-6-(1-benzimidazolylmethyl)-4-(3,5,5-trimethyl-2-pyrazolin-1-yl)-1,3,5-triazine hemihydrate	potential biological activity
EWEKAS	3-Amino-5-(1-(2-fluorobenzyl)-1H-indazol-3-yl)-10-oxa-1,4,6,8-tetra-azatricyclo(7.3.1.$0^{2,7}$)trideca-2,4,6-trien-13-ol	potent sGC-stimulator
EWUHAF01	Hydroflumethiazide	diuretic-hypertensive agent
FEDVAM	3-(N'-(4-Hydroxy-3-methoxyphenyl)methylenehydrazinocarbonyl)-1H-1,2,4-triazole	potential biological activity

FIYTEN	1-(3-C-(Ethynyl)-4-C-(hydroxymethyl)-beta-D-erythro-pentofuranosyl)cytosine	antiHIV or anticancer activity
GAHHOM	2',3'-Dideoxycytidine	agent of potential use in AIDS therapy
JABJEC	(1,2,3,4-Tetrahydro-2-naphthalenyl)methyl sulfamic acid ester	anticonvulsant activity
KECPUE	N-(Phenylamino)-2-azaspiro(4.5)decane-1,3-dione	neurotoxic activity
KEHZAY	2-Amino-7-methyl-9-(beta-D-ribofuranosyl)-8(9H)-thioxopurin-6(1H)-one monohydrate	immune system stimulatory action
LINFOD	3,5-Diamino-6-(2-methylphenyl)-1,2,4-triazine hemihydrate	analogue of lamotrigine an anticonvulsant drug
MAMMEU01	Trichotoxin A50E acetonitrile solvate hydrate	antibiotic activity
MEBQEQ01	5-Fluorocytosine	used in the treatment of fungal infections
MOPQUD	4-(Allylamino)-2-amino-6-benzyloxy-5-nitrosopyrimidine	potential in vitro inhibitor of human DNA repair protein O^6 alkylguanine-DNA-transferase
MOQLUA	Elloxazinone A	moderate inhibition of the proliferation of human cells from gastric adenocarcinoma in vitro; strong inhibition of hepatocellular carcinoma cells; no antibacterial or antifungal activity against tested organisms
NILSEG	Aqua-(sulfato)-tetrakis(urea)-magnesium	a new defoliating agent
NUJDAX	2,2'-Difluoro-2'-deoxycytosine dihydrate	antitumor activity
OFEWOL	Ethyl N-(2-amino-6-benzyloxy-5-nitrosopyrimidin-4-yl)glycinate	potential AGT inhibitor
PACMOX	2,4-Diamino-5,7-bis(butylamino)-8-fluoroquinazoline-6-carbonitrile	tested for anticancer activity
PIWVUN	cis-2-Amino-5-(benzoyl)-1-((4-nitrophenyl)sulfonyl)-4-phenyl-4,5-dihydro-1H-pyrrole-3-carbonitrile	Some antiproliferative effect (as a 1:2 cis:trans ratio of isomers) against two cancer cell lines, HeLa and MCF7/AZ, as models for human cervical and breast adenocarcinoma, respectively
POHYER	4,6-Di-O-acetyl-2,3-dideoxy-alpha-D-erythro-hex-2-enopyranosyl sulfamide	selective inhibitor of carbonic anhydrase isozyme IX
QAFRAR	5-Cyclopropyl-2-(1-(2-fluorobenzyl)-1H-pyrazolo(4,5-b)pyridin-3-yl)-4-pyrimidinamine	inhibits maximum constriction of phenylephrine-treated preconstricted rabbit aortic rings
ROLPAJ	1-Phenyl-4-(4-phthalimidobutyl)piperazine-1,4-dioxide dihydroperoxide hydrate	anxiolyic activity
RUKHAG	cis-4-Amino-1-(2-hydroxymethyl-1,3-oxathiolan-5-yl)-(1H)-pyrimidin-2-one	antiviral agent
UNEZAO	5H-Dibenz(b,f)azepine-5-carboxamide saccharin	treatment for epilepsy and trigeminal neuralgia
UNEZUI	Carbamazepine butyric acid solvate	treatment for epilepsy and trigeminal neuralgia
VEXLUF	D-N-gamma-L-Glutamyl-L-cysteine ethyl ester monohydrate	anticataractogenic activity and potential drug for liver a nd kidney diseases
VINTAN	Discodermolide 1 monohydrate	immunosuppressive and cytotoxic activity, as well as inhibiting the in vitro proliferation of cultured murine P388 leukaemia cells
VINTAN01	(+)-Discodermolide monohydrate	a potent antimitotic agent, an inhibitor of multidrug-resistant cancer lines and a potential new anticancer chemotherapeutic agent
VUHFIO	2-Ethoxybenzamide 1,2-benzothiazol-3(2H)-one 1,1-dioxide	ethenzamide is an analgesic drug

XORRUS	8-Chloro-10-phenyl-10H-pyrimido[5,4-b][1,4]benzothiazine-2,4-diamine 5,5-dioxide	antimalarial activity via inhibition of haemoglobin hydrolysis
YIZDUH	5-((4-Fluorophenyl)ethynyl)-1-((2-hydroxyethoxy)methyl)-1,2,4-triazole-3-carboxamide	anti-hepatitis C virus activity

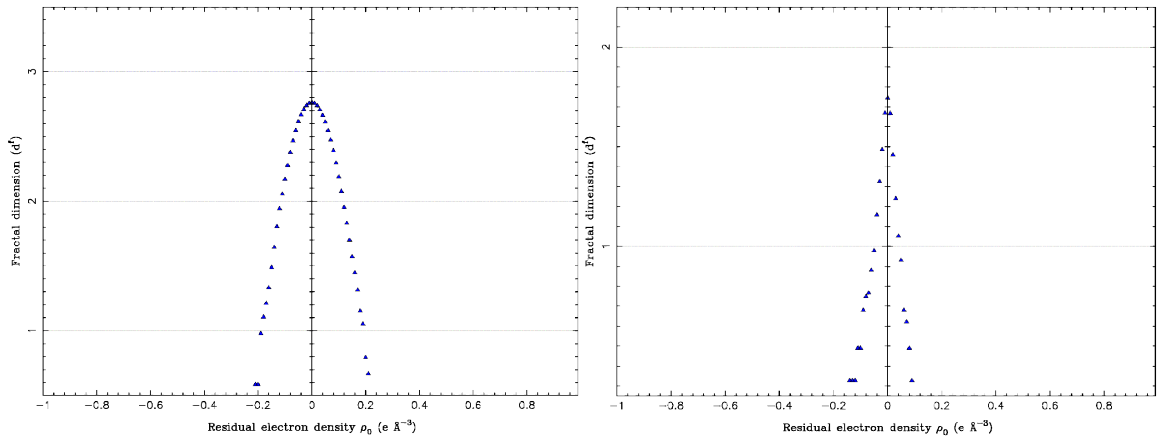

(a) **(b)**

Figure 5: Fractal dimension plot of experimental and theoretical model; (a) and (b) (**I**)

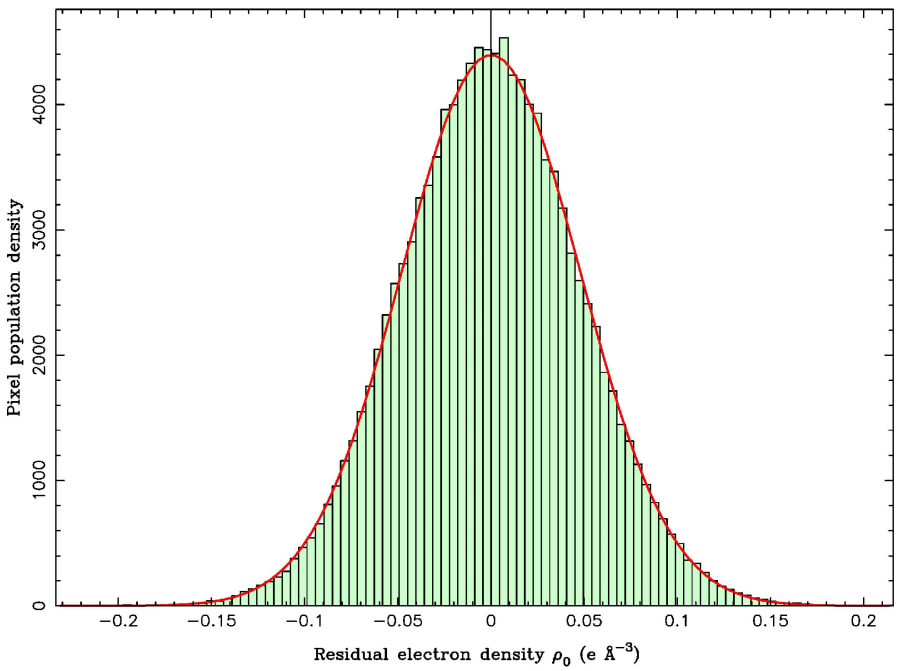

Figure 6: Probability distribution plot of experimental model

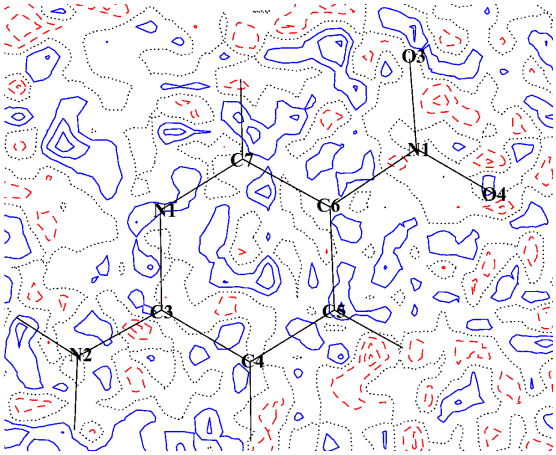
O3
C7
N1
O4
N3
C6
C3
C5
N2
C4

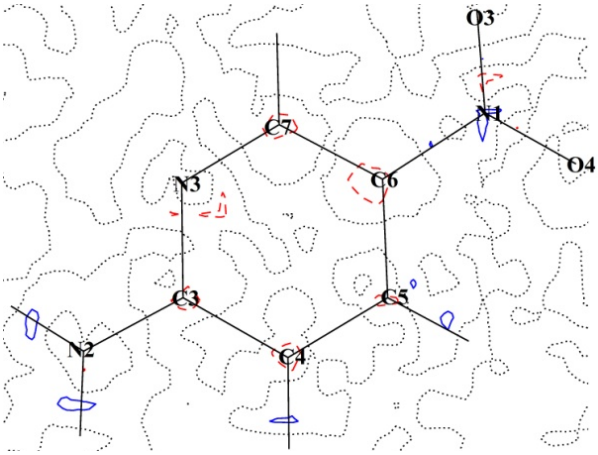
O3
C7
N1
O4
N3
C6
C3
C5
N2
C4

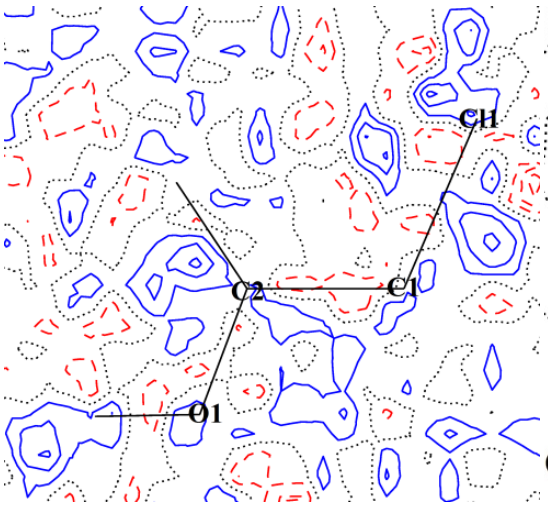
Cl1
C2
C1
O1

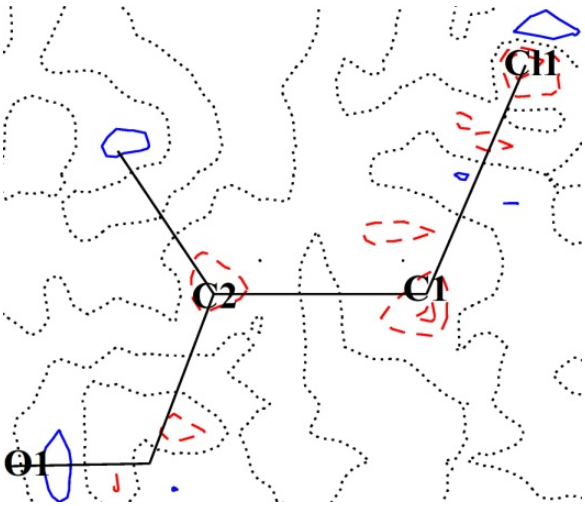
Cl1
C2
C1
O1

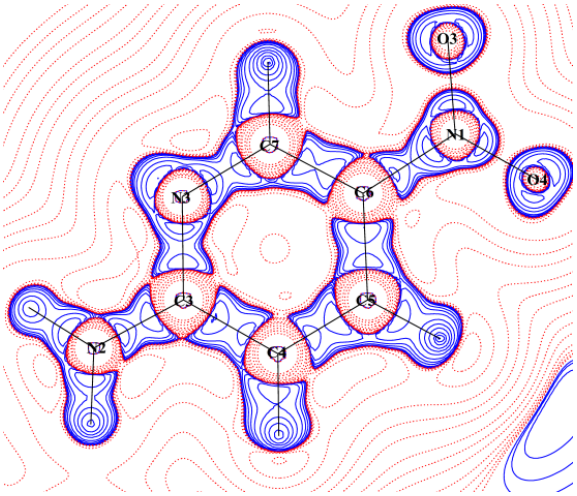
O3
C7
N1
O4
N3
C6
C3
C5
N2
C4

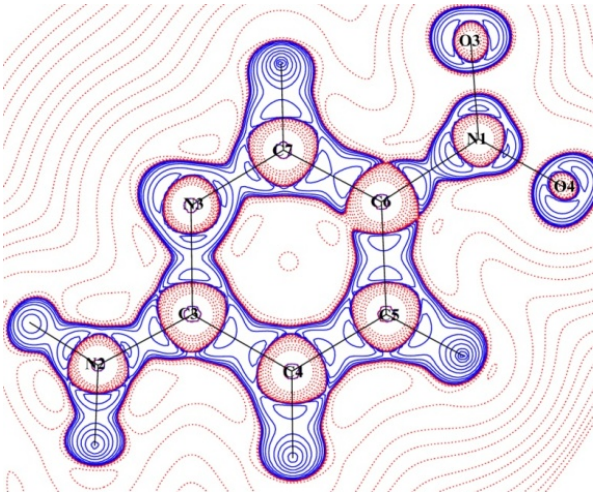
O3
C7
N1
O4
N3
C6
C3
C5
N2
C4

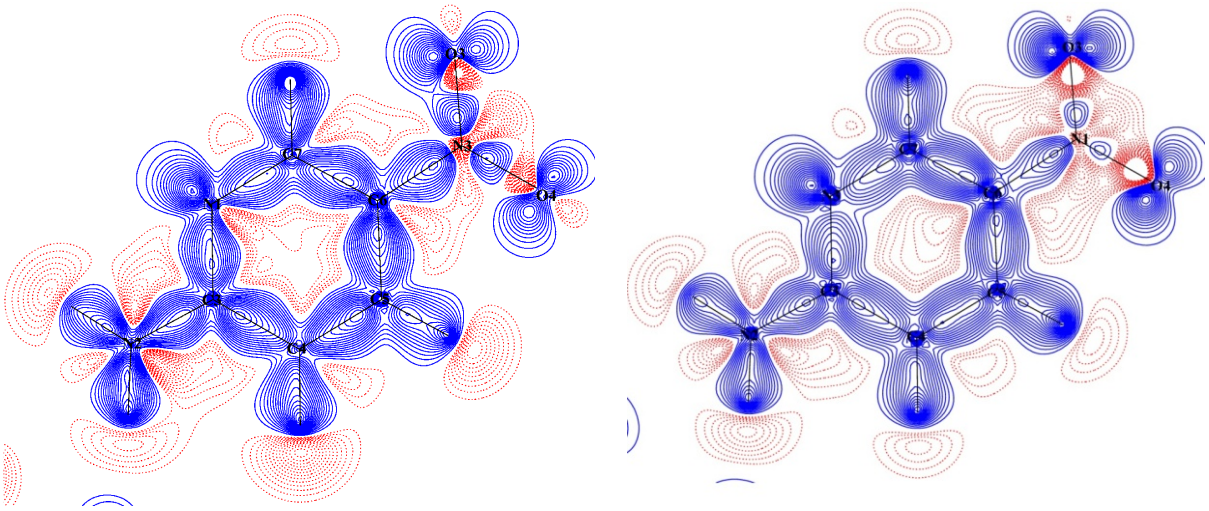

Figure 7: Experimental and Theoretical residual density, Laplacian and 2D deformation maps. Contours are drawn at the intervals of ±0.05 e $Å^{-3}$in case of residual and deformation. Laplacian is drawn in logarithmic contours.

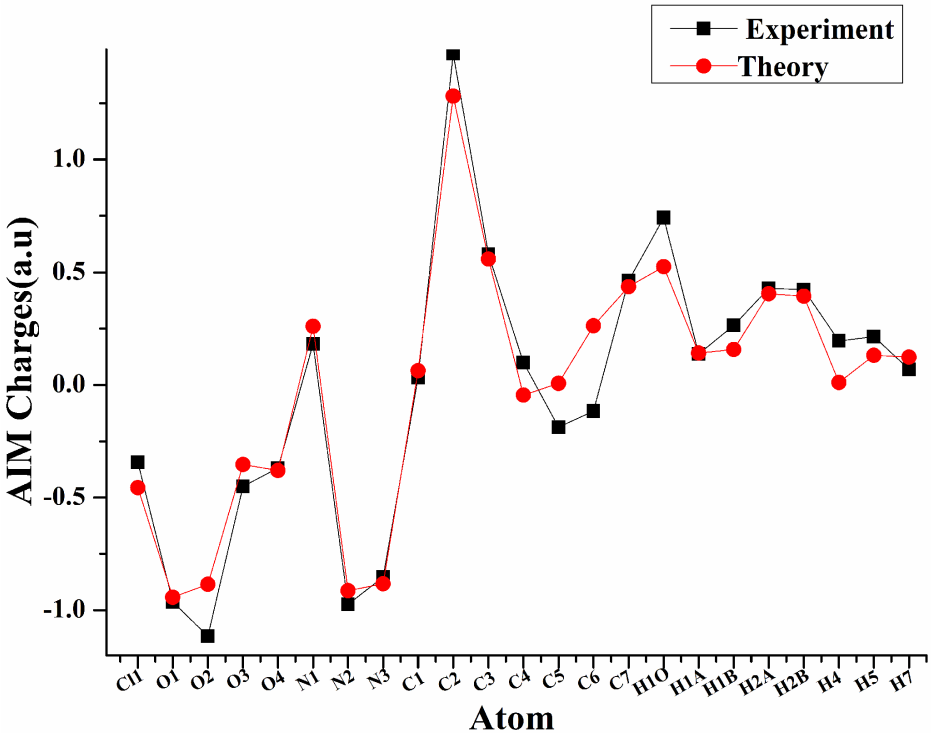

Figure 8: Comparison between experiment and theory AIM charges

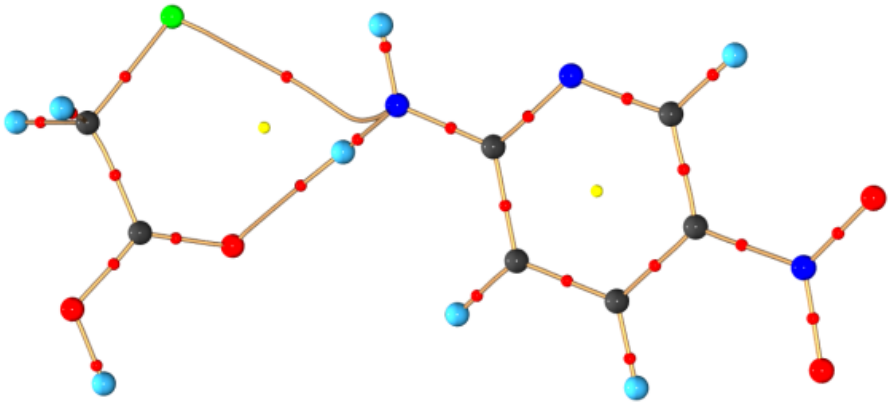

Figure 9: Theoretical bond paths together with bcp's in the intermolecular regions of (**I**)

References

1 A. Bauzá, T. J. Mooibroek and A. Frontera, *Angew. Chem. Int. Ed.*, 2013, **52**, 12317-12321.

2 R. H. Blessing, *J. Appl. Crystallogr.*, 1997, **30**, 421-426.

3 G. M. Sheldrick, *Acta Crystallogr. Sect. A: Found. Crystallogr.*, 2007, **64**, 112-122.

4 L. J. Farrugia, *J. Appl. Crystallogr.*, 2012, **45**, 849-854.

5 T. Koritsanszky, P. Macchi, C. Gatti, L. Farrugia, P. Mallinson, A. Volkov and T. Richter, *A Computer Program Package for Multipole Refinement and Topological Analysis of Charge Densities and Evaluation of Intermolecular Energies from Experimental or Theoretical Structure Factors, Version*, 2007, **5**.

6 (a)P. Macchi and P. Coppens, *Acta Crystallogr. Sect. A: Found. Crystallogr.*, 2001, **57**, 656-662; (b)Z. Su and P. Coppens, *Acta Crystallogr. Sect. A: Found. Crystallogr.*, 1998, **54**, 646-652.

7 F. H. Allen and I. J. Bruno, *Acta Crystallogr. Sect. B: Struct. Sci.*, 2010, **66**, 380-386.

8 (a)A. O. Madsen, *J. Appl. Crystallogr.*, 2006, **39**, 757-758; (b)P. Munshi, A. O. Madsen, M. A. Spackman, S. Larsen and R. Destro, *Acta Crystallogr. Sect. A: Found. Crystallogr.*, 2008, **64**, 465-475.

9 N. K. Hansen and P. Coppens, *Acta Crystallographica Section A: Crystal Physics, Diffraction, Theoretical and General Crystallography*, 1978, **34**, 909-921.

10 A. Volkov, Y. Abramov, P. Coppens and C. Gatti, *Acta Crystallogr. Sect. A: Found. Crystallogr.*, 2000, **56**, 332-339.

11 (a)C. Lee, W. Yang and R. G. Parr, *Phys. Rev. B*, 1988, **37**, 785; (b)A. D. Becke, *J. Chem. Phys.*, 1996, **104**, 1040-1046.

12 (a)A. Schäfer, H. Horn and R. Ahlrichs, *The Journal of Chemical Physics*, 1992, **97**, 2571-2577; (b)M. F. Peintinger, D. V. Oliveira and T. Bredow, *J. Comput. Chem.*, 2013, **34**, 451-459.

13 R. Dovesi, V. Saunders, C. Roetti, R. Orlando, C. Zicovich-Wilson, F. Pascale, B. Civalleri, K. Doll, N. Harrison and I. Bush, *University of Torino, Torino*, 2009.
14 A. E. Reed, L. A. Curtiss and F. Weinhold, *Chem. Rev.*, 1988, **88**, 899-926.
15 M. Frisch, G. Trucks, H. B. Schlegel, G. Scuseria, M. Robb, J. Cheeseman, G. Scalmani, V. Barone, B. Mennucci and G. Petersson, *Inc., Wallingford, CT*, 2009, **200**.
16 J.-D. Chai and M. Head-Gordon, *Phys. Chem. Chem. Phys.*, 2008, **10**, 6615-6620.
17 A. Schäfer, C. Huber and R. Ahlrichs, *J.Chem.Phys.*, 1994, **100**, 5829-5835.
18 G. Zhurko, *Chemcraft, Version 1.7 (build 365)*.